Mathematical Biosciences and Engineering

MBE, 18 (1): 112–131.
DOI: 10.3934/mbe.2021006
Received: 13 June 2020
Accepted: 10 November 2020
Published: 19 November 2020

http://www.aimspress.com/journal/MBE

Review

Pharmacokinetics and pharmacodynamics of therapeutic antibodies in tumors and tumor-draining lymph nodes

Eric Salgado[1] and Yanguang Cao[1,2,*]

[1] Division of Pharmacotherapy and Experimental Therapeutics, UNC Eshelman School of Pharmacy, University of North Carolina, Chapel Hill, NC, USA
[2] Lineberger Comprehensive Cancer Center, School of Medicine, University of North Carolina at Chapel Hill, NC, USA

* **Correspondence:** Email: yanguang@email.unc.edu.

Abstract: The signaling axis from the primary tumor to the tumor-draining lymph node (TDLN) has emerged as a crucial mediator for the efficacy of immunotherapies in neoadjuvant settings, challenging the primary use of immunotherapy in adjuvant settings. TDLNs are regarded as highly opportunistic sites for cancer cell dissemination and promote further spread via several primary tumor-dependent mechanisms. Lesion-level mixed responses to antibody immunotherapy have been traced to local immune signatures present in the TDLN and the organ-specific primary tumors that they drain. However, the pharmacokinetics (PK) and biodistribution gradients of antibodies in primary tumors and TDLNs have not been systemically evaluated. These concentration gradients are critical in ensuring adequate antibody pharmacodynamic (PD) T-cell activation and/or anti-tumor response. The current work reviews the knowledge for developing physiologically-based PK and pharmacodynamic (PBPK/PD) models to quantify antibody biodistribution gradients in anatomically distinct primary tumors and TDLNs as a means to characterize the clinically observed heterogeneous responses to antibody therapies. Several clinical and pathophysiological considerations in modeling the primary tumor-TDLN axis, as well as a summary of both preclinical and clinical PK/PD lymphatic antibody disposition studies, will be provided.

Keywords: monoclonal antibody (mAb); tumor-draining lymph nodes (TDLNs); physiologically-based pharmacokinetic (PBPK) models; target-mediated drug disposition (TMDD); PK/PD modeling

1. Introduction

1.1. General oncology therapeutic antibody pharmacokinetics

Therapeutic monoclonal antibody (mAb) therapy has exhibited remarkable success over the past decade: not only did mAb-based therapeutics account for four of the top five best-selling drugs in 2018, but the Nobel Prize in Physiology and Medicine was awarded that same year for the discovery of the mAb-based cancer immunotherapy agent ipilimumab [1,2]. Over 500 mAbs are currently being sponsored for clinical trial studies across several disease types, with cancer as the most common indication: approximately 70% of mAbs in Phase I trials are for oncological indications [3].

Antibodies are vastly larger than small molecule drugs with a molecular weight of approximately 145 kDa, and in contrast to small molecules, are generally less toxic due to their exceptional specificity to target antigens [4]. Due to their size, antibodies are generally restricted to the extracellular space (i.e., vascular and interstitial) and thus, have low volumes of distribution in humans (5–6 L) [5]. Not only are they much larger, they usually remain in circulation for long periods of time ($t_{1/2}$~3 weeks), mainly due to the presence of the neonatal Fc receptor (FcRn). FcRn recycling of IgG antibodies, which includes all of the therapeutic antibodies on the market, prevents their degradation in the intracellular lysosomal compartment and can facilitate antibody translocation through cells [5]. In terms of administration, therapeutic antibodies are most commonly delivered either intravenously (IV) or subcutaneously. Limitations of IV dosing, such as discomfort to the patient and an increased number of clinical visits, render the subcutaneous (SC) route an increasingly popular option for mAb delivery While the specific mechanisms governing mAb absorption via SC injection are not completely understood, subcutaneous delivery of mAbs and eventual distribution to the systemic circulation is proposed to be largely dependent on the uptake (i.e., drainage) via the local lymphatic vasculature (i.e., lymphatic capillaries/vessels, lymph nodes) surrounding the injection site [6,7]. Therefore, the lymphatic system plays an indispensable role in the absorption, distribution, target accumulation, and elimination properties of mAbs.

1.2. Overview of the lymphatic system (i.e., lymphatic vessels and lymph nodes) and its relevance to cancer

1.2.1 Lymphatic vessels and lymph node networks

The lymphatic system is a highly complex, multifaceted organ system whose overall main functions are to drain local tissue waste fluid (i.e., lymph) back into the circulation as well as provide host immune defense against foreign pathogens and/or abnormal (i.e., cancerous) cells [8]. It is comprised of an intricate network of lymphoid organs and tissues, including the lymphatic vasculature and lymph nodes interspersed throughout that drain fluid from surrounding tissues. When antibodies are delivered subcutaneously, they first become exposed to the interstitial space of the hypodermis, which is highly vascularized by both blood and lymphatic capillaries [9]. While FcRn-dependent mAb transcytosis through the blood capillary endothelial cell into circulation is possible, drainage via lymphatic capillaries is the primary mechanism of mAb transport out of the injection site interstitial space [9]. Generally speaking, once drained by the lymphatic capillaries, mAbs will travel through various lymph node networks (joined by larger lymphatic vessels) before

converging to a central duct, and ultimately, into the systemic circulation (Figure 1). Unlike the circulatory system, the lymphatic system has no central pump; therefore, it must rely on interstitial fluid buildup (to initiate the drainage cascade) along with local muscle contraction to effectively circulate lymph back into the systemic circulation [10]. As a result, lymph flow is dramatically slower than blood flow; on average, 500x slower (0.2% of blood flow) [11], which contributes to the long peaking time (T_{max} = 2–14 days) in the absorption of mAbs after subcutaneous dosing [12].

The various lymph node networks scattered throughout the body serve as immune checkpoints to survey local tissue for foreign pathogens or cancerous cells in draining lymph. Naïve lymphocytes (T- and B- cells), which are of bone marrow origin, travel through the bloodstream and reside in lymph nodes. Once presented with antigen from afferent lymph, these lymphocytes can induce an immune response [8]. Therapeutic antibodies are also subject to this same route for distribution; a generalized schematic of the mAb lymphatic drainage pathway is shown in Figure 1 below. The co-localizations of antibodies and lymphocytes are critical for antibodies to trigger the effector functions in the tumor-draining lymph nodes (TDLNs) for tumor eradication, which may be interrupted by surgery and the removal of TDLNs, dampening the activation of the immune system by antibodies and anti-tumor efficacy.

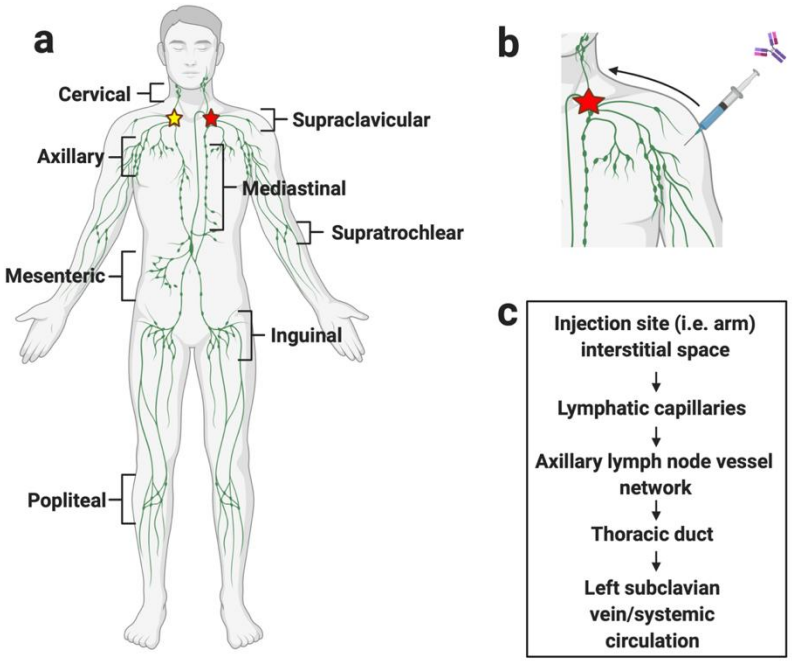

Figure 1. Generalized lymphatic drainage map and transit of therapeutic antibodies after either intravenous or subcutaneous administration. (a) Lymph node clusters (green dots), scattered throughout the body, drain lymph from surrounding tissues and into one of two subclavian veins (yellow and red stars). Lymphatic drainage is asymmetrical; the right lymph duct (yellow star) drains the right side of the head and neck, right arm/upper right core, whereas the thoracic duct (red star) drains the entire remainder of the body. (b) The flow after subcutaneous administration to the upper left arm is dependent on the (c) local system lymphatics to reach the systemic circulation.

As shown in Figure 1, lymphatic drainage in the human body is asymmetrical; a disproportionate amount of total lymph (~75%) is drained into the left thoracic duct [13]. However, a study by Xu et al in 2010 showed that the SC injection site did not significantly impact the absorption of golimumab in healthy subjects, suggesting it may not be necessary to stratify by anatomical region from a modeling perspective [14]. Furthermore, in addition to providing local tissue fluid and immune homeostasis, the lymph node clusters also vary greatly in the number, size, and even in their local immune signature (i.e., "immunostats") [15]. A table mapping the lymph node clusters draining various organs is summarized in Table 1; the lymph network structure and cluster density are critical to understanding the distribution of immunotherapies as well as their immune activation efficacy.

Table 1. Lymphatic drainage pathway by organ, along with literature reported estimates of number and size (if available). LN = lymph nodes.

Organ	Major LN drainage network	Number	Size
Brain	Cervical	300 [16]	0.48 mL (volume) [16]
Lung	Mediastinal	225 [17]	~12.6 x 8.3 mm [17]
Breast	Axillary	20–50 [18]	<10 mm (diameter) [18]
Skin	Variable	---	---
Kidney	Aortic	30–50 [19]	5–8 mm (diameter) [19]
Liver	Hepatic	30–50 [20]	3–5 mm (diameter) [20]
GI	Mesenteric	100–150 [21]	3–5 mm (diameter) [20]

1.2.2. Roles of lymphatic system and nodes (i.e., tumor-draining lymph nodes, TDLNs) in cancer

While the lymphatic vasculature and nodes play a vital role in tissue fluid/immune homeostasis, it is also highly exploited in cancers [22]. At its core, cancer is a disease of genetic instability; tumors acquire the ability to evade host immune response via immunosuppressive mechanisms in the tumor microenvironment. Moreover, a significant contributor to cancer lethality is the ability to invade (i.e., metastasize) to distal organ and tissue sites. Metastasis through the lymphatic system (as opposed to systemic blood circulation) is observed in four out of every five melanomas and carcinomas [22]. Not only does the lymphatic vasculature provide a physical basis for metastatic spread, but the lymph nodes that directly drain primary tumors (i.e., tumor-draining lymph nodes, TDLNs) become a highly opportunistic, metastatic site. Tumors generally aggregate as highly compact, hypoxic clusters of cells exerting high interstitial pressure; this high pressure is proposed to be a contributing mechanism to the dissemination of cancer cells to the TDLN [23]. Furthermore, both the primary tumor and TDLN have been shown to induce lymphangiogenesis (i.e., formation of new lymphatic vessels) to promote both local and distal metastatic spread; alarmingly, the presence of tumor cells in the TDLN was not a requirement for TDLN-mediated lymphangiogenesis. This is instead mediated by vascular endothelial growth factor A (VEGF-A) secreted by the primary tumor, which once drained via the lymphatic capillaries and is in the TDLN, induces lymphangiogenesis distally. However, once metastasized to the TDLN, cancer cells are able to promote further lymphatic vessel formation into an increasingly greater number of distal lymph nodes and tissues [24]. Moreover, rather than elicit an anti-tumor immune response, quite paradoxically, TDLNs promote both local and systemic tolerance to tumor-derived antigens. Increasing evidence has shown that the

functional activity of antigen-presenting cells (APCs) in the TDLN, along with enhanced tumor-protective host regulatory T-cell (T_{reg}) activation, promotes a tolerizing rather than immunogenic effect [25]. In light of these findings, mAb immunotherapies aiming to reverse tumor-mediated immunosuppression such as the anti-PD-1 mAb pembrolizumab have been developed and have shown great promise across a broad spectrum of cancers (Figure 2). In fact, both the primary tumor and the TDLN have been heavily implicated as a focal point for mAb immunotherapy via mechanisms that will be explained in a later section.

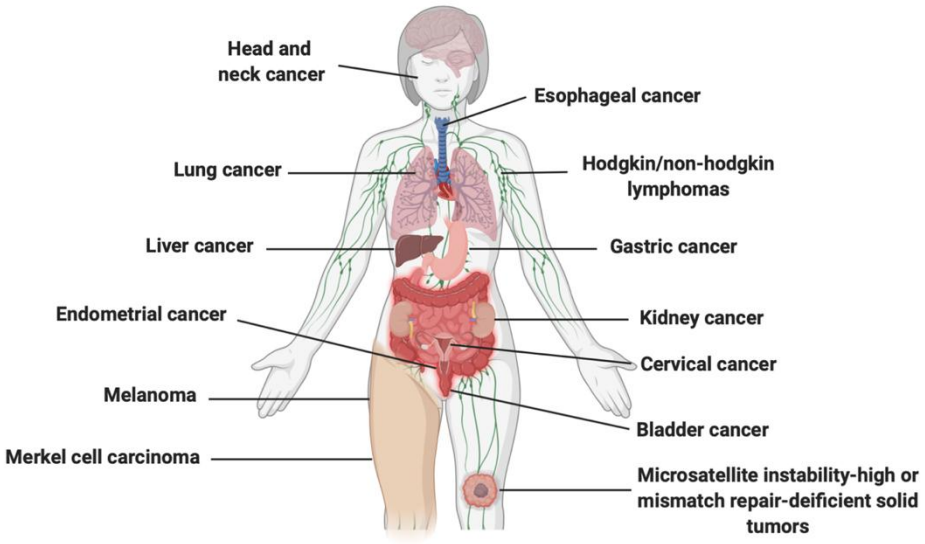

Figure 2. FDA-approved anti-PD-1 pembrolizumab cancer indications (2019) [26].

A second fundamental principle of cancer describes its disease progression as a microevolutionary process; cancer cells are continually outcompeting their neighbors for resources. Those acquiring mutations conferring a selective advantage will predominate over other sub-clones (i.e., survival of the fittest). Over time, this will create a heterogeneous lesion profile even within the same patient; as tumors metastasize to distal organs, a complex interplay between the tumor microenvironment and the local immune profile (i.e., organ-specific immunostats) further exacerbates this heterogeneity. This is reflected in the variability of response of individual lesions to pembrolizumab [27]. In this study, Osorio et al analyzed individual lesions from patients with metastatic non-small cell lung cancer (NSCLC) and mismatch repair deficiency (MMRD) carcinoma treated with PD-1 monotherapy, including pembrolizumab. CT scans of patients treated with PD-1 therapy, an immunosuppressive protein expressed in T-cells, were analyzed at the lesion level via the Response Evaluation Criteria in Solid Tumors (RECIST) v1.1 criteria to evaluate individual lesion pattern of progression. More specifically, the RECIST v1.1 criteria assesses changes in overall patient tumor burden upon treatment using specific response metrics. Predetermined guidelines and tumor shrinkage cut-offs are used to denote whether a tumor has achieved no, partial, or complete response. These metrics may then be correlated to disease progression endpoints such as progression-free survival (PFS) and overall survival (OS) [28]. Results revealed a site-specific difference in response to treatment; lymph node lesions tended to show the greatest response, while bone and liver metastases were among the least responsive [27]. These results strongly suggest that

immunologic response is not homogenous and there may likely be organ-specific factors at play influencing the level of response. Furthermore, these results also argue against the pooling of individual patient lesions to summarize overall disease progression, the current procedure for RECIST v1.1 analyses [28]. Given the established role of TDLNs in influencing both local and systemic tolerance to tumor antigens, the unique TDLN networks draining their anatomically distinct primary tumors become a highly attractive target for further exploration.

1.3. PK/PD modeling as a tool to evaluate mAb disposition and binding in individual tumors & TDLNs

Arguably, the lymphatic vasculature in the context of cancer progression is understudied, and its role in influencing mAb PK/PD remains largely unknown. As previously mentioned, one of the most common routes of mAb administration (i.e., subcutaneous injections) is partly dependent on transit via local lymphatic vessels and lymph nodes for entry into the systemic circulation. Thus, the findings mentioned above substantiate the need to develop a platform that systematically analyzes individual, inherently heterogeneous tumors, and those metastasized to TDLNs via lymphatic vessels, while accounting for mAb disposition and binding at each of these lesion sites. PK/PD modeling provides a quantitative exploration of antibody disposition at the lesion level. It offers the potential to model and simulate several clinically relevant scenarios that would otherwise be extremely costly to evaluate experimentally [29]. The following section will discuss modeling approaches, such as physiologically-based pharmacokinetic (PBPK) and target-mediated drug disposition (TMDD) modeling, to assess therapeutic antibody disposition and binding to both primary tumors and TDLNs. A summary of preclinical PK/PD mAb lymphatic distribution studies and the extrapolation of preclinical mAb PBPK approaches to clinical studies will also be provided.

2. Modeling mAb disposition and binding in the primary tumor, lymphatic vasculature

2.1. Physiologically-based pharmacokinetic (PBPK) models

PBPK modeling provides a powerful, quantitative opportunity to investigate organ and tissue-specific processes that contribute to mAb disposition and binding in both primary tumors and TDLNs. At its core, PBPK modeling aims to incorporate physiologically-relevant parameters, such as the anatomical volumes of lymph nodes and the tumor-specific lymph flow, to characterize a relatively complete PK footprint of the relevant system [30]. This is in contrast to conventional mammillary models where the lumped compartments used to describe the systemic drug PK, rather than drug disposition in target tissues, do not carry much physiological relevance (Figure 3).

As shown in Figure 3, typical PBPK models emphasize blood flow whereas lymph flow is secondary. While both flows have been accounted for in previously published models [31–33], in the context of antibody disposition/binding to both primary tumors and lymph nodes, anatomically distinct tumors are ignored and instead lumped into a “tumor” compartment; lymph nodes are also lumped together and antibody binding to antigens in the lymph nodes has not yet been investigated. From a mass balance perspective, previous PBPK models provided a useful approach to capture whole-body antibody disposition; however, tumor and lymph node specificity is sacrificed. Thus, a novel approach to emphasize mAb binding and disposition to organ-specific primary tumors as well

as to their draining lymph nodes must be considered. Our group is currently investigating these questions by utilizing existing positron electron tomography (PET) imaging clinical data (Section 2.4) to build a tumor-specific/TDLN PBPK model. This will be critical in understanding the concentration gradient between these two tissues, while also assessing if antibody can achieve sufficient exposure for full immune activation not only in the primary tumors but also in the TDLNs. Therefore, the following section will compartmentalize the primary tumor-TDLN axis and will describe the differential equations necessary to quantify antibody disposition at these tissue sites.

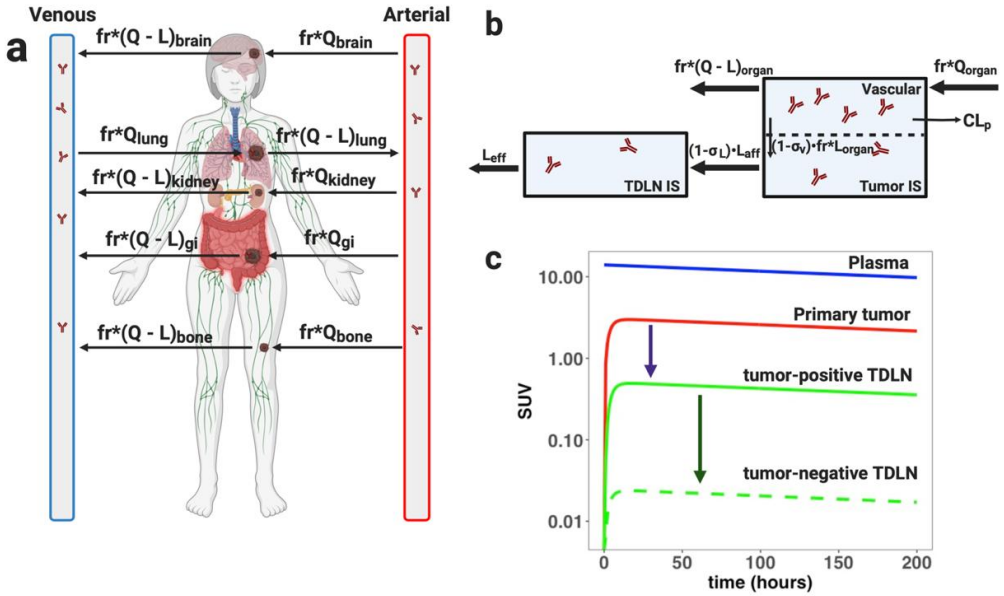

Figure 3. PBPK modeling allows for evaluation of mAb disposition and binding in tumor-specific organs and TDLNs. (a) A series of mass-balance differential equations describing the time course of antibody concentrations in both primary tumors (PT) and TDLNs are derived and implemented into the model; every organ-specific primary tumor and TDLN serves as its own physiological compartment. Typically, these compartments are connected via blood flow (black arrows), and lymph flow (green structures) is secondary; however, when considering antibody disposition, the lymphatic vasculature must be emphasized. Fr denotes the flow fraction of blood/lymph to a given tissue (i.e., tumors), which varies across tissues, tumor types/sizes, and tumor vascular structure. **(b)** Tissue- and organ-specific schematic and model parameters in primary tumors and TDLNs: Organ blood flow (Q_{organ}), vascular reflection coefficient ($\boldsymbol{\sigma}_v$), lymphatic reflection coefficient ($\boldsymbol{\sigma}_L$), afferent lymph flow (L_{aff}), efferent lymph flow (L_{eff}), organ lymph flow (L_{organ}), mAb clearance from central compartment (CL_p), interstitial space (IS). Green circular structures denote T-cells in both tumor and TDLN IS compartments interacting with draining antibody. (c) Example simulation illustrating antibody disposition (SUV, standard uptake value) in plasma (blue), primary tumor (red), tumor-positive TDLN (solid green), and tumor-negative TDLN (dashed green). The purple and green arrows denote the concentration gradients between PT-TDLN and the effect of antibody binding in the TDLN, respectively (i.e., metastasis to TDLN). For further exploration on PBPK models, please consult the following references [32,34,35].

2.2. Modeling antibody disposition and binding along the primary tumor-TDLN axis: model schematic, parameters, ODEs

The model structure described in Figure 4 summarizes the components involved in modeling mAb disposition and binding across both primary tumors and TDLNs. As described in the schematic, instead of using a full-body PBPK model, a simplified minimal PBPK (mPBPK) model can be applied to emphasize antibody PK in both of these tissues. In fact, mPBPK models describing antibody disposition in similar circuits have previously been described [36-39].

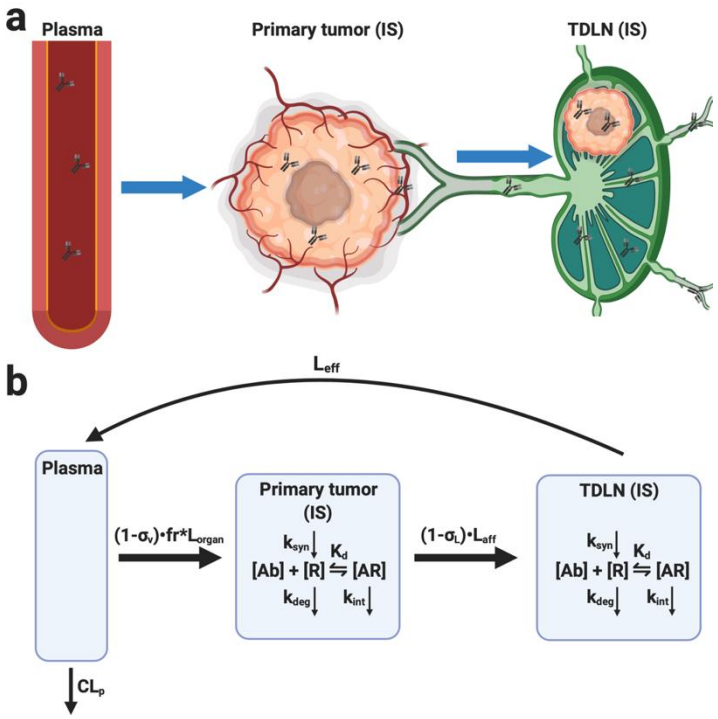

Figure 4. mPBPK model structure of antibody disposition in plasma, primary tumors and TDLNs. (a) Sequential mAb flow as it extravastates from the vascular space into the tumor interstitial space (IS), subsequently into the TDLN IS via afferent lymph flow, and then exits via efferent lymph flow. Membrane-bound antigen present at any site (i.e., tumors) will retain bound antibody, and only free (i.e., unbound) antibody will remain in circulation. (b) Antibody-antigen binding in the primary tumor IS space is described via a quasi-equilibrium target-mediated drug disposition (QE-TMDD) model. Free antibody leaving the tumor IS compartment will then travel via the lymphatic vessels to the TDLN where a second QE-TMDD model can be applied in the TDLN, assuming antigen (i.e., tumor) is present. Efferent flow will then deliver remaining antibody back into the plasma. Symbols are defined below. (Figure prepared in BioRender).

The differential equations describing the model are as follows (assuming IV injection):

$$V_p\left(\frac{dC_{Ab,p}}{dt}\right) = Input - (1 - \sigma_v) \bullet fr \bullet L_{organ} \bullet C_{Ab,p} - CL_p \bullet C_{Ab,p} + L_{eff} \bullet Cf2 \quad (1)$$

$$V_{isf_{PT}}\left(\frac{dC_{Ab,PT}}{dt}\right) = (1 - \sigma_v) \bullet fr \bullet L_{organ} \bullet C_{Ab,p} - (1 - \sigma_L) \bullet L_{aff} \bullet Cf1 - k_{int} \bullet AR_{PT} \bullet V_{isfPT} \quad (2)$$

$$\frac{dR_{PT}}{dt} = k_{syn} - k_{\deg} \bullet (R_{T,PT} - AR_{PT}) - k_{int} \bullet AR_{PT} \quad (3)$$

$$V_{isf,TDLN}\left(\frac{dC_{Ab,TDLN}}{dt}\right) = (1 - \sigma_L) \bullet L_{aff} \bullet Cf1 - L_{eff} \bullet Cf2 - k_{int} \bullet AR_{TDLN} \bullet V_{isfTDLN} \quad (4)$$

$$\frac{dR_{TDLN}}{dt} = k_{syn} - k_{\deg} \bullet (R_{T,TDLN} - AR_{TDLN}) - k_{int} \bullet AR_{TDLN} \quad (5)$$

$C_{Ab,p}$, $C_{Ab,PT}$, and $C_{Ab,TDLN}$ denote antibody concentrations in the central (i.e., plasma) compartment, primary tumor (PT), and TDLN, respectively. R_{PT} and R_{TDLN} refer to total antigen concentration in primary tumor and in TDLN. Initial conditions for each differential equation are as indicated: IC($C_{ab,p}$) = Dose (assuming IV route of administration); IC($C_{Ab,PT}$) = 0; IC(R_{PT}) = ksyn/kdeg; IC($C_{Ab,TDLN}$) = 0; IC(R_{TDLN}) = ksyn/kdeg. V_p, $V_{isf,PT}$, and $V_{isf,TDLN}$ refer to plasma volume, primary tumor interstitial fluid volume, and TDLN interstitial fluid volume. L_{organ}, L_{aff}, and L_{eff} are the organ lymph flows quantifying antibody extravasation from the vasculature into the primary tumor interstitial space, as well as TDLN afferent and efferent lymph flows, respectively. CL_p is the clearance of antibody from the central compartment, and σ_v and σ_L are the vascular and lymphatic reflection coefficients. Fr denotes the flow fraction of blood/lymph to a given tissue (i.e., tumors), which varies across tissues, tumor types/sizes, and tumor vascular structure. AR_{PT} and AR_{TDLN} are bound antibody-antigen concentrations at these sites, defined by the following equations:

$$AR_{PT} = \frac{R_{T,PT} \bullet Cf1}{K_d + Cf1} \quad (6)$$

$$AR_{TDLN} = \frac{R_{T,TDLN} \bullet Cf2}{K_d + Cf2} \quad (7)$$

Therapeutic antibodies have been shown to undergo a phenomenon known as target-mediated drug disposition (TMDD), whereby the exceptionally high affinity for antibody to an antigen, along with limited target capacity, influences its pharmacokinetic properties [40]. For membrane-bound targets, this is reflected by the internalization rate (k_{int}) of the antibody-antigen complex, followed by degradation. The TMDD structure is depicted in Figure 3 within both the primary tumor and TDLN compartments, and due to model complexity, can be simplified according to certain assumptions. A quasi-equilibrium TMDD (QE-TMDD) approximation is used here, wherein many cases, equilibrium binding (K_d) is on a much faster time-scale than the other parameters describing target synthesis (k_{syn}), degradation (k_{deg}) and internalization (k_{int}). TMDD models are constructed so that only total antibody and total receptor differential equations are required; free antibody concentrations within either the primary tumor (Cf1) or TDLN (Cf2) interstitial space are expressed as a quadratic function dependent on total antibody and total target concentrations as well as the K_d, and are defined as follows:

$$Cf1 = 0.5 \bullet \{(C_{Ab,PT} - R_{T,PT} - K_d) + \sqrt{\left(C_{Ab,PT} - R_{T,PT} - K_d\right)^2 + 4 \bullet C_{Ab,PT} \bullet K_d}\} \quad (8)$$

$$Cf2 = 0.5 \bullet \{(C_{Ab,TDLN} - R_{T,TDLN} - K_d) + \sqrt{\left(C_{Ab,TDLN} - R_{T,TDLN} - K_d\right)^2 + 4 \bullet C_{Ab,TDLN} \bullet K_d}\} \quad (9)$$

Sources for parameter values to implement in the model can be consulted in the following references [34,41]; however, it must be emphasized that the volumes and flows are largely organ- and tumor-specific. A study by Brown et al in 2019 assessed tumor-specific perfusion which can be used to calculate tumor-specific processes, such as the fr (fraction of tumor-specific lymph flow) [42]. Once built, the model and its parameters may be evaluated by utilizing PET imaging data that details antibody binding to both PT and TDLNs, as discussed in Section 2.4. There are several critical assumptions and notable observations in this model structure; as previously mentioned, due to their large size, antibodies are mainly restricted to the vascular and target site interstitial spaces and should be reflected accordingly in the differential equations. Moreover, this model structure quantifies only one primary tumor to its sentinel TDLN or the first LN that directly drains the primary tumor. It is assumed that all of the free antibody leaving the TDLN interstitial space flows directly and entirely into the central compartment. Additionally, processes such as lymphangiogenesis and FcRn-mediated salvage within the lymphatic capillaries are not accounted for in this model. Previous modeling analyses and bioavailability studies indicate that roughly 2/3 of antibody is recycled (ranging from ~52–100%) through this pathway [43]; thus, FcRn recycling must be implemented into the model if it is critical for the research question or it may be empirically included. Furthermore, as previously stated, these differential equations capture these concentration gradients after IV injection. If presented with SC data, an additional absorption compartment has to be considered; previous models have captured this process as referenced [34,43] Nonetheless, the model schematic and differential equations illustrated here provide a solid starting point for quantitative investigation of antibody disposition in primary tumors and TDLNs. The following sections will summarize the landscape of previous preclinical PK/PD antibody lymphatic studies as well as provide insights on immuno-PET imaging methods as a non-invasive way to study antibody pharmacokinetics in primary tumors and TDLNs in the clinical setting.

2.3. Preclinical antibody PK/PD lymphatic studies

While there have been several published PBPK models assessing mAb disposition in animal tumors, as previously mentioned, none to-date have analyzed lesion-level organ-specific tumor heterogeneity. Instead, these models have grouped all tumors into a "tumor" compartment, and thus, lose the ability to stratify by organ lesion type [32,33,35]. The same can be said about LNs and TDLNs; these lymphatic structures are usually secondary to blood flow, and while accounted for in the model, are seldom systemically assessed. While the scope of this review emphasizes antibody disposition in primary tumors and TDLNs, it is important to get an understanding of all of the processes that affect mAb PK at these tissue sites. As previously mentioned, subcutaneous injections are an increasingly popular route of administration for mAbs, and as such, factors such as the injection site interstitial space and lymphatic transit, among others, must be evaluated. Charman et al.

investigated causes of degradation of human growth hormone (hGH), a different class of biologics, via the lymphatics in sheep; they reported that injection site interstitial space only minimally contributed to hGH degradation. However, it was shown that overall degradation via the lymphatics contributed significantly, as only 62% of hGH was recovered in peripheral lymph from the efferent duct of the popliteal lymph nodes [44]. A subsequent analysis then demonstrated that degradation of therapeutic proteins in freshly collected lymph was also minimal in rats and dogs; however, proteolysis in the LNs was shown to contribute to decreased mAb bioavailability [45]. It is not surprising given that resident protease-secreting immune cells in the LNs can catabolize mAbs. Furthermore, the role of FcRn salvage in the lymphatic vessels is vital in maintaining intact antibody as FcRn-knockout mice are devoid of all IgG within four days; over 50% of IgG remained in wild-type mice after several days [46], consistent with the half-life of IgG antibodies. While the exact processes governing antibody lymphatic absorption remain unknown, these findings highlight various components of the lymphatic vasculature that should be considered when modeling antibody disposition in primary tumors and TDLNs.

2.4. Clinical antibody primary tumor & TDLN PK/PD studies/approaches

There are no direct clinical studies that have assessed mAb disposition in primary tumors and TDLNs. A study published by Varkhede et al. analyzed published data across several clinical mAb PK studies (in healthy volunteers) to build a minimal PBPK model to quantify mAb absorption after subcutaneous administration. They attributed a loss of antibody bioavailability to interstitial proteolysis, likely in the sentinel LNs, supporting previous findings [34]. Interestingly, they attributed antibody-specific factors as a contributing factor to the reduction in mAb absorption; physiochemical factors such as the mAb isoelectric point was shown to correlate with interstitial LN proteolysis, suggesting that factors inherent to the mAb need to be considered as well. However, a couple of limitations to this study were that actual LN concentration data was unavailable and thus was not directly calibrated or assessed. Furthermore, this model was not optimized in a cancer setting.

Several studies have used immuno-PET imaging as a non-invasive way to quantify antibody uptake and binding across various tissues, including primary tumors and TDLNs [47-49]. Immuno-PET imaging takes advantage of a radiolabeled tracer (^{89}Zr-, ^{64}Cu-, etc.) on the mAb and is able to quantify whole-body antibody biodistribution *in vivo* and through time. Typically, the standard uptake value (SUV) is used as the quantitative indicator of uptake. It is simply a ratio of the target organ/tissue radioactivity divided by whole-body radioactivity, normalized by body weight. SUV values also take into consideration the half-life of the radioisotope and are thus adjusted for time-decay. A higher SUV value denotes higher accumulation and/or binding in target tissues. Therefore, it provides an opportunity to build a PBPK framework for the investigation of antibody disposition and binding in primary tumors and TDLNs. However, some limitations with this approach include sparse sampling, limited TDLN data, and a lack of specific information on anatomical TDLNs collected. Furthermore, SUV data can be variable even with the same lesion and between scans [50]; nonetheless, these empirical values still provide a valuable resource for model calibration and analysis in the clinical setting.

3. Clinical/pathophysiological factors that can influence antibody disposition and binding in primary tumors & TDLNs

3.1. Clinical factors

3.1.1. Neoadjuvant vs. adjuvant immunotherapy

Cancer surgery undoubtedly remains the gold standard for treating tumors if "resectable for cure," and is much more tolerated than either chemotherapy or antibody therapy. However, as previously mentioned, metastases, and especially micrometastases that go unnoticed, are the overwhelming cause of cancer-related deaths. In terms of cancer mAb therapies, especially in the immunotherapy context (i.e., checkpoint blockade mAbs such as pembrolizumab), the currently accepted approach is to administer these therapies in the late-stage, adjuvant (i.e., post-primary tumor resection) setting. However, an emerging body of evidence is supporting immunotherapy administration in much earlier settings, before surgery (i.e., neoadjuvant immunotherapy); these studies are being supported across several different cancer types. A study in early-stage colon cancer revealed that 95% of mismatch repair (MMR)-deficient (dMMR) tumors treated with neoadjuvant immunotherapy exhibited major pathological response (≤10% residual viable tumor), with 60% of all lesions showing complete response (100% reduction) [51]. A study in recurrent glioblastoma showed that neoadjuvant pembrolizumab extended median progression-free survival (PFS) from 72.5 days (adjuvant group) to 99.5 days (neoadjuvant group); enhanced clonal expansion of T-cells and decreased PD-1 expression on peripheral T-cells were also reported in the neoadjuvant group [52]. Furthermore, in locally advanced melanomas, a potent and rapid anti-tumor response was observed in patients receiving neoadjuvant immunotherapy, with 8 of 27 patients experiencing a major or complete pathological response. All eight of those patients remained disease after only a single dose of pembrolizumab and were associated with T-cell reinvigoration seen as early as one-week post-treatment [12]. Collectively, these findings strongly suggest that antibody administration in the neoadjuvant setting is modulating a fundamental principle of possibly all cancers.

The primary tumor-TDLN signaling axis has been highlighted as a focal point for neoadjuvant immunotherapy success [53]; in the neoadjuvant setting, while the primary tumor is still intact, this allows for more efficient antibody-mediated pharmacodynamic T-cell priming at both the primary tumor (PT) site as well as in the TDLN due to the higher levels of endogenous tumor antigen present. Moreover, an intact PT-TDLN signaling axis will ensure an adequate antibody concentration gradient at both sites (i.e., sufficient antibody delivery at both the PT and TDLN). This enhanced systemic immunity is then better able to scavenge and eliminate micrometastases in tissues (via the intact lymphatic vasculature and the blood vasculature) that would otherwise be the source of post-surgical relapse. In the case of immunotherapy administration such as pembrolizumab, which targets the PD-1 receptor in T-cells, this will allow for an even greater reinvigoration of T-cells in the tumor microenvironment, reversing tolerance induction caused by tumor antigens such as the PD-1 receptor ligand PD-L1 [53]. However, careful attention must be paid to the timing of neoadjuvant immunotherapy and allowing adequate time for systemic immunity, as preclinical evidence shows an optimal time window before tumor burden supersedes therapeutic benefit [54]. In cases where antibody is administered post-surgery, insufficient mAb delivery (i.e., lower/inefficient biodistribution gradient) to the TDLN, due to a disruption in the local lymphatic vasculature, may

have deleterious consequences, such as micrometastatic tumor relapse/resistance. Thus, maintaining adequate mAb biodistribution gradients to the TDLN are critical in driving both antibody PK and PD response in the clinical setting.

3.1.2. Surgical resection

Sentinel lymph node (SLN) biopsies is a technique that arose in the early 1990s that is used to assess the metastatic potential of the primary tumor and involves excising surrounding proximal lymph nodes that are believed to be the first set of nodes draining the tumor. However, the controversy over the overall risk-benefit utility of this procedure has been raised throughout the years as lymphedema (swelling of the excised area due to compromised lymphatic drainage) is presented in nearly 30% of SLN patients [55]. Not only does this impede the patient's quality of life, but it also provides a further pharmacokinetic barrier of efficient antibody delivery to more distal lymph nodes surrounding the region. Furthermore, as previously mentioned in the neoadjuvant immunotherapy case, this insufficient delivery will likely result in suboptimal mAb-antigen binding found in micrometastases in the TDLN, leading to an attenuated anti-tumor response for other antibody types, such as trastuzumab.

3.1.3. Formulations

The Varkhede et al. subcutaneous lymphatic mAb absorption study that was previously discussed noted a co-formulation effect on affecting antibody PK in the interstitial space; hyaluronidase is an enzyme that is commonly co-administered with therapeutic antibodies as it helps ease discomfort with subcutaneous injections. It allows for higher mAb injection volumes. It is also known to disrupt the hyaluronic acid-dependent subcutaneous extracellular matrix present in the interstitial space, allowing for more efficient, rapid delivery [34]. Their original model only estimated the interstitial LN proteolysis (i.e., LN-mediated mAb clearance parameter, CL_{LN}) and, in doing so, overpredicted the T_{max} for those mAbs co-formulated with hyaluronidase. Once the subcutaneous injection site lymph flow rate was allowed to be simultaneously estimated with the CL_{LN} parameter, the model fits were much improved; final model estimates for the injection site lymph flow rate were markedly higher and ranged anywhere from 20- to 330- fold than the original value [34], consistent with the known pharmacology of hyaluronidase. Therefore, a detailed formulation description of the therapeutic antibody should be evaluated when modeling disposition in the lymphatic vasculature and LNs.

3.2. Pathophysiological factors

3.2.1. Inflammation

Inflammation is the body's natural response to combat pathogens and is essential for tissue immune homeostasis. However, tumor-associated inflammation, which has been proposed as the seventh hallmark of cancer [56], can make profound changes within the tumor microenvironment and in the surrounding lymphatic vasculature and TDLNs. Both pro- and anti-inflammatory cytokine release have been shown to heighten interstitial flow in the lymphatic capillaries and vessels.

Coupled with lymphatic vessel enlargement, it can drastically alter the PK of antibody delivery to both primary tumors and TDLNs [57]. Presumably, this would result in a diluting effect that could give rise to suboptimal mAb concentrations in the TDLN.

3.2.2. Spatial factors

The tumor extracellular matrix (ECM) is markedly different from healthy tissue; it is composed of a complex network of myofibroblasts, collagen and other ECM components such as hyaluronan and proteoglycans (PGs), among other components. ECM content, even within different anatomical tumors, can drastically differ [58] and can have dramatic effects on antibody disposition at these sites. These findings corroborate well with a couple of aforementioned studies; lesion-level heterogeneous responses to pembrolizumab have been previously explained and can, in part, be attributed to these anatomical differences. Furthermore, negatively-charged hyaluronan, which is overexpressed in tumors, aids in tumor invasiveness and the epithelial-mesenchymal transition (EMT) [58]. Given that many mAbs usually carry a positive charge, this might enhance electrostatic interaction and thus retain mAbs within the tumor ECM and create an even higher concentration gradient between the primary tumor and TDLN. For these reasons, antibody disposition in organ-specific primary tumors and TDLNs should be emphasized and characterized accordingly.

4. Conclusion

In summary, while largely understudied, the TDLN is an invaluable asset to the tumorigenic and metastatic cascade; it not only acts as a physical means of cancer cell dissemination but is also a dynamic regulator of both local and systemic tolerance to tumor antigens. Cancer cells are able to exploit the TDLNs in such a way that ultimately progresses, rather than prohibits, further spread. In the context of mAb therapies that depend on interstitial and lymphatic uptake to both the primary tumor and TDLN, several clinical as well as pathophysiological factors should be considered when quantitatively modeling this axis. While seemingly identical in shape and universal in function, organ-specific immuno-regulation can vastly influence the local immune signature, which can differentially affect antibody responses to anatomically distinct lesions. The work described here has provided a PBPK/TMDD modeling approach to successfully characterize mAb disposition in organ-specific primary tumors as well as in the TDLNs that drain them. Future clinical studies should take advantage of immuno-PET imaging methods and emphasize distinct TDLN networks throughout the body to predict antibody disposition at these sites more reliably.

Acknowledgments

This research is supported by NIH grant GM119661.

Conflict of interest

The authors declare no conflicts of interest. E.S. is a postdoctoral fellow sponsored by the UNC/IQVIA fellowship.

References

1. M. Brooks, Cancer Drugs Dominate Top 10 Best-Selling Drugs in 2018, *Medscape Medical News*, March 19, 2019.
2. Press release: The Nobel Prize in Physiology or Medicine 2018, In: *NobelPrize.org*, 2018.
3. R.-M. Lu, Y.-C. Hwang, I. J. Liu, C.-C. Lee, H.-Z. Tsai, H.-J. Li, et al., Development of therapeutic antibodies for the treatment of diseases, *J. Biomed. Sci.*, **27** (2020), 1.
4. H. M. Shepard, G. L. Phillips, C. D Thanos, M. Feldmann, Developments in therapy with monoclonal antibodies and related proteins, *Clin. Med. (Lond)*, **17** (2017), 220–232.
5. N. L. Dirks, B. Meibohm, Population Pharmacokinetics of Therapeutic Monoclonal Antibodies, *Clin. Pharmacokinet.*, **49** (2010), 633–659.
6. D. N. McLennan, C. J. H. Porter, G. A. Edwards, S. W. Martin, A. C. Heatherington, S. A. Charman, Lymphatic Absorption Is the Primary Contributor to the Systemic Availability of Epoetin Alfa following Subcutaneous Administration to Sheep, *J. Pharmacol. Exp. Ther.*, **313** (2005), 345.
7. A. Supersaxo, W. R. Hein, H. Steffen, Effect of molecular weight on the lymphatic absorption of water-soluble compounds following subcutaneous administration, *Pharm. Res.*, **7** (1990), 167–169.
8. L. N. Cueni, M. Detmar, The lymphatic system in health and disease, *Lymphat. Res. Biol.*, **6** (2008), 109–122.
9. H. Zhou, F. P. Theil, ADME and translational pharmacokinetics/pharmacodynamics of therapeutic proteins, *Gut*, **60** (2015), 774 ‐ 779.
10. J. E. Moore, Jr., C. D. Bertram, Lymphatic System Flows, *Ann. Rev. Fluid. Mech.*, **50** (2018), 459–482.
11. C. O'Driscoll, *Lymphatic Transport of Drugs*, 1992.
12. A. C. Huang, R. J. Orlowski, X. Xu, R. Mick, S. M. George, P. K. Yan, et al., A single dose of neoadjuvant PD-1 blockade predicts clinical outcomes in resectable melanoma, *Nat. Med.*, **25** (2019), 454–461.
13. K. N. Margaris, R. A. Black, Modelling the lymphatic system: challenges and opportunities, *J. Roy. Soc. Interface*, **9** (2012), 601–612.
14. Z. Xu, Q. Wang, Y. Zhuang, B. Frederick, H. Yan, E. Bouman-Thio, et al., Subcutaneous Bioavailability of Golimumab at 3 Different Injection Sites in Healthy Subjects, *J. Clin. Pharmacol.*, **50** (2010), 276–284.
15. W. Pao, C.-H. Ooi, F. Birzele, A. Ruefli-Brasse, M. A. Cannarile, B. Reis, et al., Tissue-Specific Immunoregulation: A Call for Better Understanding of the "Immunostat" in the Context of Cancer, *Cancer Discov.*, **8** (2018), 395.
16. M. Ying, B. S. Pang, Three-dimensional ultrasound measurement of cervical lymph node volume, *Br. J. Radiol.*, **82** (2009), 617–625.
17. G. M. Glazer, B. H. Gross, L. E. Quint, I. R. Francis, F. L. Bookstein, M. B. Orringer, Normal mediastinal lymph nodes: number and size according to American Thoracic Society mapping, *AJR Am. J. Roentgenol.*, **144** (1985), 261–265.
18. F. Maxwell, C. de Margerie Mellon, M. Bricout, E. Cauderlier, M. Chapelier, M. Albiter, et al., Diagnostic strategy for the assessment of axillary lymph node status in breast cancer, *Diagn. Interv. Imaging*, **96** (2015), 1089–1101.

19. R. E. Dorfman, M. B. Alpern, B. H. Gross, M. A. Sandler, Upper abdominal lymph nodes: criteria for normal size determined with CT, *Radiology*, **180** (1991), 319–322.
20. M. Taupitz, Imaging of Lymph Nodes — MRI and CT. In: Hamm B, Forstner R, editors. *MRI and CT of the Female Pelvis*. Berlin, Heidelberg: Springer Berlin Heidelberg. (2007), 321–329.
21. E. A. Abdel Gawad, M. F. Abu Samra, A. M. Talat, The utility of multi-detector CT in detection and characterization of mesenteric lymphadenopathy with histopathological confirmation, *Egypt. J. Radiol. Nucl. Med.*, **47** (2016), 757–764.
22. S. P. Leong, E. K. Nakakura, R. Pollock, M. A. Choti, D. L. Morton, W. D. Henner, et al., Unique patterns of metastases in common and rare types of malignancy, *J. Surg. Oncol*., **103** (2011), 607–614.
23. S. Chandrasekaran, M. R. King, Microenvironment of tumor-draining lymph nodes: opportunities for liposome-based targeted therapy, *Int. J. Mol. Sci.*, **15** (2014), 20209–20239.
24. S. Hirakawa, S. Kodama, R. Kunstfeld, K. Kajiya, L. F. Brown, M. Detmar, VEGF-A induces tumor and sentinel lymph node lymphangiogenesis and promotes lymphatic metastasis, *J. Exp. Med.*, **201** (2005), 1089–1099.
25. T. J. Curiel, S. Wei, H. Dong, X. Alvarez, P. Cheng, P. Mottram, et al., Blockade of B7-H1 improves myeloid dendritic cell-mediated antitumor immunity, *Nat. Med.*, **9** (2003), 562–567.
26. K. Honey, Use of Pembrolizumab Expanded to 13th Type of Cancer in Five Years, In: Catalyst CR, editor: American Association for Cancer Research. (2019).
27. J. C. Osorio, K. C. Arbour, D. T. Le, J. N. Durham, A. J. Plodkowski, D. F. Halpenny, et al., Lesion-Level Response Dynamics to Programmed Cell Death Protein (PD-1) Blockade, *J. Clin. Oncol.*, **37** (2019), 3546–3555.
28. L. H. Schwartz, S. Litière, E. de Vries, R. Ford, S. Gwyther, S. Mandrekar, et al., RECIST 1.1-Update and clarification: From the RECIST committee, *Eur. J. Cancer*, **62** (2016), 132–137.
29. K. Feng, R. H. Leary, Toward personalized medicine with physiologically based pharmacokinetic modeling, *Int. J. Pharmacokinet.*, **2** (2016), 1–4.
30. I. Nestorov, Whole-body physiologically based pharmacokinetic models, *Expert Opin. Drug Metab. Toxicol.*, **3** (2007), 235–249.
31. S. R. Urva, V. C. Yang, J. P. Balthasar, Physiologically based pharmacokinetic model for T84.66: a monoclonal anti-CEA antibody, *J. Pharm. Sci.*, **99** (2010), 1582–1600.
32. L. Abuqayyas, J. P. Balthasar, Application of PBPK modeling to predict monoclonal antibody disposition in plasma and tissues in mouse models of human colorectal cancer, *J. Pharmacokinet. Pharmacodyn.*, **39** (2012), 683–710.
33. D. K. Shah, A. M. Betts, Towards a platform PBPK model to characterize the plasma and tissue disposition of monoclonal antibodies in preclinical species and human, *J. Pharmacokinet. Pharmacodyn.*, **39** (2012), 67–86.
34. N. Varkhede, M. L. Forrest, Understanding the Monoclonal Antibody Disposition after Subcutaneous Administration using a Minimal Physiologically based Pharmacokinetic Model, *J. Pharm. Pharm. Sci.*, **21** (2018), 130s–148s.
35. K. L. Gill, I. Gardner, L. Li and M. Jamei, A Bottom-Up Whole-Body Physiologically Based Pharmacokinetic Model to Mechanistically Predict Tissue Distribution and the Rate of Subcutaneous Absorption of Therapeutic Proteins, *Aaps J.*, **18** (2016), 156–170.

36. Y. Cao, W. J. Jusko, Incorporating target-mediated drug disposition in a minimal physiologically-based pharmacokinetic model for monoclonal antibodies, *J. Pharmacokinet. Pharmacodyn.*, **41** (2014), 375–387.
37. Y. Cao, J. P. Balthasar, W. J. Jusko, Second-generation minimal physiologically-based pharmacokinetic model for monoclonal antibodies, *J. Pharmacokinet. Pharmacodyn.*, **40** (2013), 597–607.
38. Y. Cao, W. J. Jusko, Applications of minimal physiologically-based pharmacokinetic models, *J. Pharmacokinet. Pharmacodyn.*, **39** (2012), 711–723.
39. B. M. Maas, Y. Cao, A minimal physiologically based pharmacokinetic model to investigate FcRn-mediated monoclonal antibody salvage: Effects of Kon, Koff, endosome trafficking, and animal species, *mAbs*, **10** (2018), 1322–1331.
40. D. E. Mager, W. J. Jusko, General pharmacokinetic model for drugs exhibiting target-mediated drug disposition, *J. Pharmacokinet. Pharmacodyn.*, **28** (2001), 507–532.
41. P. R. V. Malik, A. Hamadeh, C. Phipps, A. N. Edginton, Population PBPK modelling of trastuzumab: a framework for quantifying and predicting inter-individual variability, *J. Pharmacokinet. Pharmacodyn.*, **44** (2017), 277–290.
42. L. V. Brown, E. A. Gaffney, A. Ager, J. Wagg, M. C. Coles, Comparative Anatomical Limits of CART-Cell Delivery to Tumours in Mice and Men, *bioRxiv* (2019), 759167.
43. L. Zhao, P. Ji, Z. Li, P. Roy, C. G. Sahajwalla, The Antibody Drug Absorption Following Subcutaneous or Intramuscular Administration and Its Mathematical Description by Coupling Physiologically Based Absorption Process with the Conventional Compartment Pharmacokinetic Model, *J. Clin. Pharmacol.*, **53** (2013), 314–325.
44. S. A. Charman, A. M. Segrave, G. A. Edwards, C. J. Porter, Systemic availability and lymphatic transport of human growth hormone administered by subcutaneous injection, *J. Pharm. Sci.*, **89** (2000), 168–177.
45. W. Wang, N. Chen, X. Shen, P. Cunningham, S. Fauty, K. Michel, et al., Lymphatic transport and catabolism of therapeutic proteins after subcutaneous administration to rats and dogs, *Drug. Metab. Dispos.*, **40** (2012), 952–962.
46. R. P. Junghans, C. L. Anderson, The protection receptor for IgG catabolism is the beta2-microglobulin-containing neonatal intestinal transport receptor, *Proc. Natl Acad. Sci. USA*, **93** (1996), 5512.
47. C. W. Menke-van der Houven van Oordt, A. McGeoch, M. Bergstrom, I. McSherry, D. A. Smith, M. Cleveland, et al., Immuno-PET Imaging to Assess Target Engagement: Experience from (89)Zr-Anti-HER3 mAb (GSK2849330) in Patients with Solid Tumors, *J. Nucl. Med.*, **60** (2019), 902–909.
48. R. de Bree, J. C. Roos, J. J. Quak, W. den Hollander, A. J. Wilhelm, A. van Lingen, et al., Biodistribution of radiolabeled monoclonal antibody E48 IgG and F(ab')2 in patients with head and neck cancer, *Clin. Cancer Res.*, **1** (1995), 277–286.
49. J. E. Mortimer, J. R. Bading, J. M. Park, P. H. Frankel, M. I. Carroll, T. T. Tran, et al., Tumor Uptake of (64)Cu-DOTA-Trastuzumab in Patients with Metastatic Breast Cancer, *J. Nucl. Med.*, **59** (2018), 38–43.
50. P. E. Kinahan, J. W. Fletcher, Positron emission tomography-computed tomography standardized uptake values in clinical practice and assessing response to therapy, *Semin. Ultrasound CT MR*, **31** (2010), 496–505.

51. M. Chalabi, L. F. Fanchi, K. K. Dijkstra, J. G. Van den Berg, A. G. Aalbers, K. Sikorska, et al., Neoadjuvant immunotherapy leads to pathological responses in MMR-proficient and MMR-deficient early-stage colon cancers, *Nat. Med.*, **26** (2020), 566–576.
52. T. F. Cloughesy, A. Y. Mochizuki, J. R. Orpilla, W. Hugo, A. H. Lee, T. B. Davidson, et al., Neoadjuvant anti-PD-1 immunotherapy promotes a survival benefit with intratumoral and systemic immune responses in recurrent glioblastoma, *Nat. Med.*, **25** (2019), 477–486.
53. S. L. Topalian, J. M. Taube, D. M. Pardoll, Neoadjuvant checkpoint blockade for cancer immunotherapy, *Science*, **367** (2020), eaax0182.
54. J. Liu, S. J. Blake, M. C. Yong, H. Harjunpää, S. F. Ngiow, K. Takeda, et al., Improved Efficacy of Neoadjuvant Compared to Adjuvant Immunotherapy to Eradicate Metastatic Disease, *Cancer Discov.*, **6** (2016), 1382–1399.
55. H. Assi, E. Sbaity, M. Abdelsalam, A. Shamseddine, Controversial indications for sentinel lymph node biopsy in breast cancer patients, *Biomed. Res. Int.*, **2015** (2015), 405949–405949.
56. F. Colotta, P. Allavena, A. Sica, C. Garlanda and A. Mantovani, Cancer-related inflammation, the seventh hallmark of cancer: links to genetic instability, *Carcinogenesis*, **30** (2009), 1073–1081.
57. M. A. Swartz, A. W. Lund, Lymphatic and interstitial flow in the tumour microenvironment: linking mechanobiology with immunity, *Nat. Rev. Cancer*, **12** (2012), 210–219.
58. H. Wiig, M. A. Swartz, Interstitial fluid and lymph formation and transport: physiological regulation and roles in inflammation and cancer, *Physiol. Rev.*, **92** (2012), 1005–1060.

Supplementary

1. R code for the proposed PBPK model (for simulation use in RxODE)

```
############################################################
odeex <- "
Cp = centr/Vp # central compartment
CTtumor = tumor/Visf #primary tumor compartment
CTtdln = tdln/Vtdln #tumor-positive TDLN
CTtdln2 = tdln2/Vtdln #tumor-negative TDLN

#SUV (STANDARD UPTAKE VALUE CALCULATION: SUV = CONCENTRATION (NMOL/L)*WHOLE-BODY VOLUME (L)/INJECTED DOSE (NMOL))
SUVpl = Cp*70/34.6
SUVtm = CTtumor*70/34.6
SUVtd = CTtdln*70/34.6
SUVtd2 = CTtdln2*70/34.6

#CONCENTRATION OF FREE ANTIBODY IN PT (Cf1), TUMOR-POSITIVE TDLN (Cf2), TUMOR-NEGATIVE TDLN (Cf3)

Cf1 = 0.5*((CTtumor - tumRec - Kd) + ((CTtumor - tumRec - Kd)^2 + 4*CTtumor*Kd)^0.5)
Cf2 = 0.5*((CTtdln - tdlnRec - Kd) + ((CTtdln - tdlnRec - Kd)^2 + 4*CTtdln*Kd)^0.5)
```

```
Cf3 = 0.5*((CTtdln2 - tdlnRec2 - Kd) + ((CTtdln2 - tdlnRec2 - Kd)^2 + 4*CTtdln2*Kd)^0.5)

#RECEPTOR OCCUPANCY
AT1 = tumRec*Cf1 / (Kd + Cf1)
AT2 = tdlnRec*Cf2 / (Kd + Cf2)
AT3 = tdlnRec2*Cf3 / (Kd + Cf3)

#FRACTION OF LYMPH FLOW THAT IS TUMOR-SPECIFIC (VARIES WIDELY ACROSS TUMOR TYPES)
fr = 0.00353

d/dt(centr) = - (1 - sigmav)*Lorgan*Cp*fr - CLp*Cp + L2*Cf2 + L2*Cf3
d/dt(tumor) = (1 - sigmav)*Lorgan*Cp*fr - (1 - sigmal)*Cf1*L1 - (1 - sigmal)*Cf1*L1 - AT1*kint*Visf
d/dt(tdln) = (1 - sigmal)*L1*Cf1 - L2*Cf2 - AT2*kint*Vtdln
d/dt(tdln2) = (1 - sigmal)*L1*Cf1 - L2*Cf3 - AT3*kint*Vtdln
d/dt(tumRec) = kdeg*R01 - kdeg*(tumRec - AT1) - AT1*kint
d/dt(tdlnRec) = kdeg*R02 - kdeg*(tdlnRec - AT2) - AT2*kint
d/dt(tdlnRec2) = kdeg*R03 - kdeg*(tdlnRec2 - AT3) - AT3*kint
"

mbex <- RxODE(odeex)

#Vp = plasma volume (L), Visf = primary tumor-specific interstitial fluid volume (L), Vtdln = TDLN interstital fluid volume (L),
#Kd = binding affinity (nM), sigmav = vascular reflection coefficient, sigmal = lymphatic reflection coefficient,
#R01/R02/R03 = antigen concentration in PT/tumor positive TDLN/tumor negative TDLN(i.e., tumor burden, nM),
#Lorgan = organ lymph flow (L/hr), CLp = antibody clearance (L/hr), L1/L2 = afferent/efferent lymph flows (L/hr),
#kint = target internalization rate (hr-1), kdeg = target degradation rate (hr-1)
params <- c(Vp = 5, Visf = .0002, Vtdln = 0.0002, Kd = 5, sigmav = 0.95, R01 = 500, R02 = 100, R03 = 0,
            Lorgan = .0815, CLp = .009, L1 = .004, L2 = .004, sigmal = 0.2, kint = 0.01, kdeg = 0.01)
inits <- c(0, 0, 0, 0, 500, 100, 0)

ev <- eventTable()
ev$add.dosing(dose = 34.6, nbr.doses = 1, dosing.to = 1)
ev$add.sampling(0:200)
#dose = nmol

reviewsim <- as.data.frame(mbex$solve(params, ev, inits), stiff = TRUE)
```

reviewsim

```
s100 <- ggplot(reviewsim,aes(time,SUVpl)) + geom_line(col="blue", cex = 1.5) +
   geom_line(col="red",dat=reviewsim,aes(time,SUVtm),cex = 1.5) +
   geom_line(col="green",dat=reviewsim,aes(time,SUVtd),cex = 1.5) +
   geom_line(col="green",dat=reviewsim,aes(time,SUVtd2),cex = 1.5, lty=2) + ylab("SUV") +
xlab("time (hours)") + theme_bw() +
   theme(axis.title.x = element_text(family="sans", face="bold", size=18)) +
   theme(axis.title.y = element_text(family="sans", face="bold", size=18)) +
   theme(axis.text.x = element_text(family="sans", face="bold", size=18)) +
   theme(axis.text.y = element_text(family="sans", face="bold", size=18)) +
   theme(panel.grid.major = element_blank(), panel.grid.minor = element_blank()) +
   scale_y_log10()
s100
############################################################
```

2. Determination of "fr" (fraction of organ blood/lymph flow to tumor): Kidney example

Tumor perfusion to kidney[42]: 240 mL/min/100g
Assuming a 1 cm^3 (= 1 mL = 1 g) tumor:

$$Q_{kidney,tumor} = \left(\frac{240\ mL/min}{100\text{g}}\right) * 1g = 2.4\ mL/min$$

Assuming lymph is 0.002 blood flow (1/500):

$\frac{2.4ml/min}{500}$ = 0.288 mL/hr = 0.000288 L/hr (tumor-specific kidney lymph flow)

Normal kidney blood flow = 40.75 L/hr

$\frac{40.75L/hr}{500} = 0.0815\ L/hr$ (normal kidney lymph flow, Lorgan)

Lorgan*fr = Lkidney tumor

0.0815 L/hr * fr = 0.000288 L/hr

fr = 0.003533742